Iranica Journal of Energy & Environment
Journal Homepage: www.ijee.net
IJEE an official peer review journal of Babol Noshirvani University of Technology, ISSN:2079-2115

Photocatalytic Degradation of Sulfamethoxazole in Visible Irradiation Using Nanosized $NiTiO_3$ Perovskite

S. Jain* and U. Chandrawat

Department of Chemistry, Govt. P.G. College, Kota 324001, India

P A P E R I N F O

Paper history:
Received 12 February 2018
Accepted in revised form 10 April 2018

Keywords:
Pechini synthesis
$NiTiO_3$
Photodegradation
Sulfamethoxazole

A B S T R A C T

Nickel titanium oxide ($NiTiO_3$) nanoparticles were synthesized at low temperature in non aqueous medium by modified Pechini method using ethylene glycol and citric acid as polymeric precursors. The structural and morphological characteristics of the products were studied by X-ray diffraction, fourier transform infrared spectroscopy (FT-IR), UV-Visible diffuse reflectance spectroscopy (UV-DRS), scanning electron microscope (SEM) and energy dispersive X-ray spectroscopy (EDAX). XRD patterns of powder revealed crystalline rhombohedral $NiTiO_3$ obtained at 700 ◦ C and this crystalinity increased with temperature. SEM images estimated that the grain sizes of $NiTiO_3$ to be in the range 10–250 nm. DRS spectra reveal two peaks, one at around 440-450 nm and another one at around 740-750 nm. The band gap energy was calculated using Tauc plot and it was found to be 1.67 eV. In this study, photocatalytic properties of $NiTiO_3$ on sulfamethoxazole drug degradation was investigated which has not been reported elsewhere and results shows that it is a prominent material for photodegradation of drug in the range of visible light.

***doi**: 10.5829/ijee.2017.09.01.05*

INTRODUCTION

Human pharmaceutical and their metabolites are discharged by sewage treatment plants to river, lake, and seawater. Numerous studies have shown that the pharmaceutical residues are widespread in the aquatic environment [1-3]. Sulfonamide antibiotics are one of the oldest classes of antimicrobial agents among the administered antibiotic compound classes and frequently used in European countries and Korea. Derivatives of sulphanilamide drugs are used in aquaculture, animal husbandry and human medicine to treat bacterial infections [4]. Sulfamethoxazole (SMX) is one of the most widely prescribed sulphonamide drugs. It is only partly removed in conventional sewage treatment plant effluent and it has been found in effluent from wastewater treatment plants in concentration varying from 0.01 to 2 µg/L in many countries. It has been also found in drinking water. There is, therefore, a need to develop efficient treatments for these effluents [5-7].

Recently, Advanced Oxidation Processes (AOPs) based on generation of strongly reactive hydroxyl radicals (∗OH) have received a large interest for the removal of pharmaceuticals from waste water [8-10]. Among the AOPs, heterogeneous photocatalysis is considered as a promising process for pharmaceuticals active ingredients treatment operating under ambient temperature and pressure [11-15].

The best approach to realize visible-light photocatalysis is to develop a new photocatalytic material independent of TiO_2. Oxide materials are plausible candidates of the new photocatalytic material in relation to their high chemical stability and easy preparation compared with non-oxide materials. Kim et al. [16], Kudo et al. [17] and Tang et al. [18] recently reported several doped and undoped oxide photocatalyst responsive to visible light. However, their activities for drugs degradation are not sufficient yet at wavelengths longer than 500 nm. Recently, special attention has been paid to the titanium –based ilmenites, $MTiO_3$, as chemical, electrical and optical materials because of their excellent ferroelectric, dielectric and electro-optical properties [19-21]. Nickel titanate ($NiTiO_3$) belongs to the ilmenite type structure with both Ni and Ti possessing octahedral coordination and the alternating cation layers occupied by Ni^{+2} and Ti^{+4} alone. Ilmenite $NiTiO_3$ has a wide range of application such as electrodes of solid oxide fuel cells, metal-air barriers, gas sensors, tribological coating, corrosion inhibitors, pigments, electronic material in electrochemical energy storage devices and so on due to their high static dielectric constants, weak magnetism and semiconductivity. $NiTiO_3$, as a semiconductor has excellent photocatalytic

* Corresponding author: Seema Jain
E-mail: jay4seema@yahoo.co.in

activity due to its absorption band [22-25]. There are numerous reports regarding the investigations on the photocatalytic activity of $NiTiO_3$, like degradation of Tergitol, Sfranine T and Rhodamine B [26, 27]. Moreover, the properties of $NiTiO_3$ depend on its preparation method. $NiTiO_3$ nanostructured powder with ilmenite – type structure can be obtained by solid-state reaction, wet chemical solution, combustion electrospinning, polymeric precursor, precipitation, and sol-gel methods. The main disadvantage of the conventional approaches is calcination of the powder mixture at high temperatures ranging from 1100 to 1300 ^oC; the coarse- grained powder synthesized by these methods contain agglomerated particles of different size with impure phase due to incomplete synthesis reaction. It still remains a challenge for the scientific community to obtain quality $NiTiO_3$ nanoparticles at a low temperature while avoiding unwanted by-product. The polymeric citrate precursor route has been used earlier [28, 29] for the synthesis of NTO particles. Success of above synthesis encouraged us to use some modification at our end by using non aqueous medium to obtain $NiTiO_3$ particles with a controlled morphology, narrow size distribution and high purity through the Pechini type reaction route at low temperature and utilize it in sulpha drug degradation.

In the literature, a lot of studies focused on SMX photocatalysis by UV light; however, it is to be noted that natural systems are exposed to atmospheric sunlight which has not gained much attention. Furthermore, transformations products (TPs) of SMX photocatalysis by visible light were mostly not considered. The main aim of this work is to investigate the TPs formed during photolcatalysis and prove the efficiency of synthesized $NiTiO_3$ in the degradation of SMX in the visible light.

MATERIAL AND METHODS

Materials

Nickel chloride ($NiCl_2$), titanium tetraisopropoxide $Ti\{OCH(CH_3)_2\}_4$, citric acid ($C_6H_8O_7$) and ethylene glycol ($C_2H_6O_2$) were purchased from Merck (India). Sulfamethoxazole was purchased from Sigma-Aldrich. Deionized water was used in all the experiments.

Synthesis of $NiTiO_3$ perovskite

$NiTiO_3$ perovskite was prepared from polymeric precursors method proposed by Pechini method. Firstly, stoichiometric amount of Titanium tetraisopropoxide was added to 56.1 gm of ethylene glycol. The mixture was stirred on a magnetic stirrer for 15 min and heated up to 80 ^oC to get clear transparent solution. At this stage, citric acid (CA) was added in a ratio of 4:1 with respect to metal ion and 60:40 (w/w) with respect to ethylene glycol. A white precipitate was observed immediately after adding citric acid to the solution but it dissolved after stirring the solution for 5 min. The contents were stirred at 80 ^oC till a clear solution was obtained. After that stoichiometric amount of nickel chloride was dried in an oven for 2 h and added to the ethylene glycol - citric acid – Ti isopropoxide solution prepared as above. The contents were stirred on a magnetic stirrer till the nickel chloride dissolve and continue the heating on hot plate, a yellowish resin was formed. The obtained resin was polymerized at 300 ^oC for 2 h at a heating rate of 2 ^oC/min in air. The resulting black sponge polymer was calcined in air at 600 ^oC, 700 ^oC and 800 ^oC for 4 h at 2 ^oC /min. A yellowish crystalline ceramic powder was obtained thereafter.

Characterization

Several techniques were used for characterization of the powders. Thermal gravimetric analyses were carried out in a TGA-7 Perkin-Elmer balance under an air flow of 50 ml min^{-1}. The maximum temperature was set to 900 ^oC and the heating rate to 5 ^oC min^{-1}. Powder X-ray diffraction (Siemens D5000 diffractometer) analyses were carried out using Cu Kα radiation at 2θ angles from 0^o to 80^o with scan speed of $5^o min^{-1}$. The vibration spectra were characterized by FTIR (FTS 7000 series, DIGILIB). The Ultraviolet and visible diffuse reflection spectra (carry 5000 absorption spectrometer) were measured at 240-800 nm wavelengths. The morphology of the samples was observed with a scanning electron microscope (SEM) (Hitachi X650, Japan).

Catalytic activity

Photodegradation experiments were performed with a photocatalytic reactor system. This bench-scale system consisted of a cylindrical Pyrex-glass cell with 1.5 L capacity (12 cm inside diameter and 15 cm height and a reflective interior surface). A 500 W Xe arc lamp (intensity 137mWcm^{-2}) lamp was placed in a 5 cm diameter quartz tube with one end tightly sealed by a Teflon stopper. The lamp and the tube were then immersed in the photoreactor cell. The photoreactor containing the prepared pervoskite was filled with 1L aqueous SMX drug solution. The whole reactor was cooled with a water cooled jacket on its outside and the temperature was kept at 25 $\pm$ 2 ^oC. During the entire experiment, mixture were magnetic stirred for keeping the solution chemically uniform and free contact with air. During SMX treatment, natural pH (5.5) was used, and this value was maintained during all experimental runs.

After the appropriate irradiation time samples were collected from the reactor and centrifuged (10 min, 4000 RPM). Before and after irradiation, the concentration of SMX in mixture was determined using HPLC-UV with a C-18 column (5 µm, 250 mm x 4.6 mm, Hypersil, USA) and diode array detector. The mobile phase was 70% of acetonitrile and 30% of milli-Q water at a flow rate of 1.0 mL min^{-1}. The detection wavelength was set at 270 nm.

Finally, the photocatalytic activities were determined using the following formula:

$$\text{Drug removal (\%)} = \frac{Co-Ct}{Co} \times 100 \quad (1)$$

where, C_o (mgL^{-1}) and C_t (mgL^{-1}) are the initial concentration of solution and the concentration after photocatalytic degradation by photocatalyst, respectively.

Total organic carbon (TOC) was measured using a multi N/C 3000 TOC analyzer (Analytik Jena AG, Germany) to evaluate the mineralization of SMX. Identification of SMX degradation products was achieved with the aid of LC-MS (ThermoQuest LCQ DUO, USA) with a C-18 HPLC column.

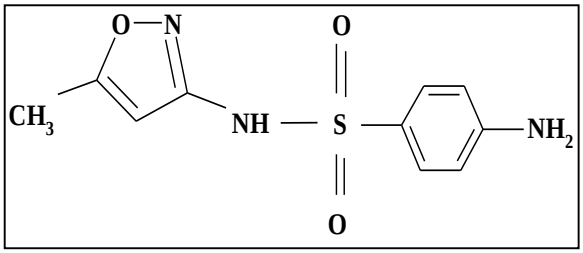

Figure 1. Molecular structures of Sulfamethoxazole drug.

RESULTS AND DISCUSSION

Characterization of $NiTiO_3$ perovskite

The decomposition process of the polymeric resin was monitored by TGA / DTA as shown in Fig.2. The TGA curve shows three main regions, the first one is mostly due to dehydration and evaporation of organic matters from 70 to 230 ^{o} C. The other large one between 230 to 500 ^{o} C seems to be associated with decomposition and burn out of the organic components. In the last stage, in the temperature range 500 to 700 ^{o} C, small weight change occurs due to the crystallization of the sample and subsequent conversion to the perovskite phase. No weight loss was observed above 700 ^{o} C indicating complete removal of organic residues and good thermal stability of crystalline $NiTiO_3$ at this temperature which can then be used finally as a photocatalyst in drug degradation. The proposed decomposition pathway for the synthesized $NiTiO_3$ has been given below:

$$MTi(C_6H_5O_7)_2 \rightarrow MTi(OH)_2(C_2O_4)_2 \rightarrow MTiO(C_2O_4)_2 \rightarrow MTiO_3 \ (M= Ni)$$

In the Fig.2 the DTA curve reveals three main endothermic events at 180.81, 355.85 and 422.04 ^{o} C. The peak at 180.81^{o} C was assigned to dehydration and depolymerisation of the polymeric residual in the precursor. Apparently, the endothermic peak at 355.85 ^{o}C was explained by the complex decomposition and combustion of the polymeric resin. The third endothermic peak at 422.04 ^{o}C could be due to the decomposition of the organic components.

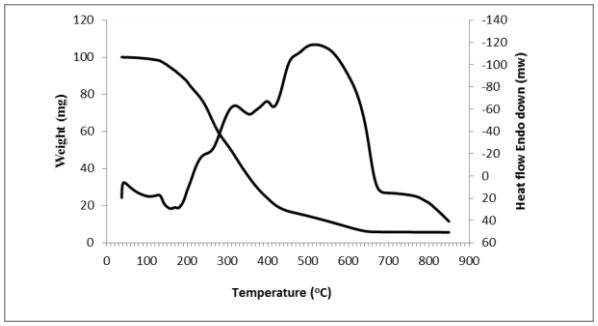

Figure 2. TGA and DTA analysis of the thermal decomposition of $NiTiO_3$ precursor resin in air (25 ^{o} – 800 ^{o}C / 5 ^{o}Cmin^{-1}) .

The crystalline structure and phase purity of the prepared powder samples were analysed using X-ray diffraction technique. Figure 3 presents the XRD patterns of $NiTiO_3$ powder calcined at different temperature ranging from 600 to 800 ^{o}C for 4 h. The powder formed at 600 ^{o}C is poor crystalline material, whereas the samples formed at 700 and 800 ^{o}C are well crystalline materials as supported by the results of TGA. The observe diffraction pattern was matched with standard data [30] and tabulated in Table 1. The crystal structure of $NiTiO_3$ is rhombohedral and the d-line pattern matched with reported ones (JCPDS file number 33-960). The average crystalline sizes were determined from XRD pattern according to the Scherrer's equation:

$$D = \frac{K\lambda}{\beta \cos \theta}$$

where D is the average crystalline size, K is a constant equal to 0.9, λ is the X-ray wavelength (0.154 nm for Cu Kα), β is the half – peak width (FWHM) and Θ is the Bragg diffraction angle. Using this approach it was estimated that the average crystallite size of the synthesized product is about 22.04, 23.03 and 32.43 nm for the sample prepared at temperature 600 ^{o}C (2Θ: 33.07, FWHM: 0.393), 700 ^{o}C (2Θ: 33.07, FWHM: 0.376) and 800 ^{o}C (2Θ: 33.04, FWHM: 0.267) respectively. The crystalline sizes clearly reveal that with increasing calcinations temperature, the crystalline size also increases.

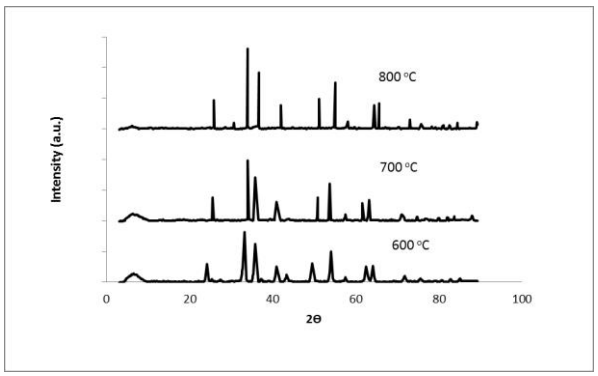

Figure 3. XRD pattern of $NiTiO_3$ at different temperature.

TABLE 1. Experimental and JCPDS data diffraction peak position of the rhombohedral $NiTiO_3$ phase for 700 ºC/4h

Phase	hkl	Lit. 2Θ	Exp. 2Θ	Lit. d (Aº)	Exp. d (Aº)
$NiTiO_3$	(012)	24.13	24.09	3.685	3.690
	(104)	33.08	33.04	2.705	2.708
	(110)	35.65	35.61	2.516	2.519
	(113)	40.85	40.80	2.207	2.209
	(024)	49.44	49.39	1.841	1.843
	(116)	54.01	53.93	1.696	1.698
	(214)	62.44	62.39	1.485	1.486
	(300)	64.06	64.01	1.452	1.453
	(1010)	71.65	71.65	1.315	1.315

FTIR analysis was carried out for detecting the presence of the functional groups and also used in order to prove that the synthesized powders are carbonate – free. FT-IR spectrum of the NTO are shown in Fig. 4. It is well known that the characteristic vibration bands corresponding to (M-O) metal –oxygen bonds will be range of 400-800 cm^{-1} [31]. The absorption peak at 544 cm^{-1} is attributed Ni-O bond and 436 cm^{-1} peak related to Ti-O bond. The characteristic bands of the carbonate (867, 1067 and 1440 cm^{-1}) are not appearing in the spectrum, it can be stated that the synthesized nano crystals are carbonate free. Therefore FT-IR spectrum confirms the formation of pure $NiTiO_3$ nano particles.

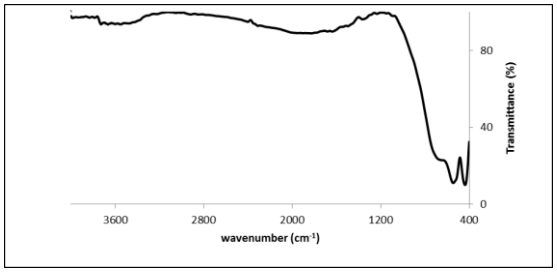

Figure 4. FTIR spectra of the $NiTiO_3$ perovskite (700 ºC/4 h).

Morphological investigation of the $NiTiO_3$ powder has been carried out using high resolution scanning electron microscopy. The SEM images at different magnificence show that the particles of $NiTiO_3$ are homogeneous, various crystal size and remarkably varying morphology. The powder exhibits particles in combination of spheroid, ellipsoid, and some hexagonal morphology. The coalescence of the particles shows range from 50 to 250 nm. The difference between the particle sizes indicates the presence of agglomerates, which is a normal phenomenon in the Pechini method. These particles are smaller than those produced by molten salt method (about 300 nm) [32], modified solid state reaction method (sintered at above 1000 ºC with comparatively large particle size about 1 µ) [33] and conventional solid-state method [34] (sintered at above 1225 ºC and particle size about 15-35 µm) again it is proved that modified Pechini method is good for synthesis of $NiTiO_3$.

To confirm the chemical composition of the synthesized $NiTiO_3$, powder was examined by EDAX analysis. The spectrum in Fig. 6 reveals the presence of Ni, Ti and O peaks confirming the formation of pure powder with no other elemental impurities. The average atomic percentage ratio of Ni:Ti:O were 20:20:60 in the 700 ºC/4 h annealed powder indicating the stoichiometric formation of $NiTiO_3$. This EDAX spectrum confirms that the targeted chemical composition could be achieved in the powder.

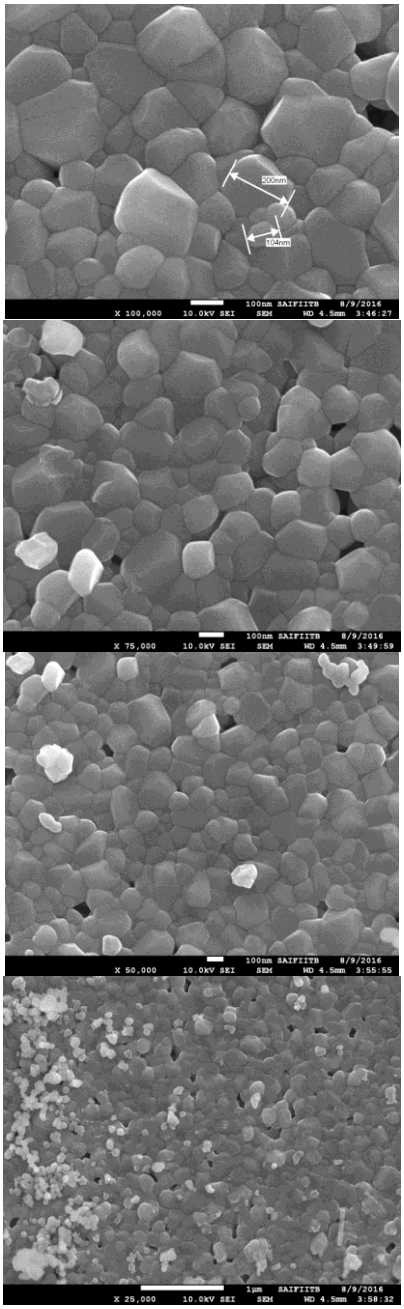

Figure 5. SEM images of $NiTiO_3$ perovskite (700 ºC/4 h) at different magnification.

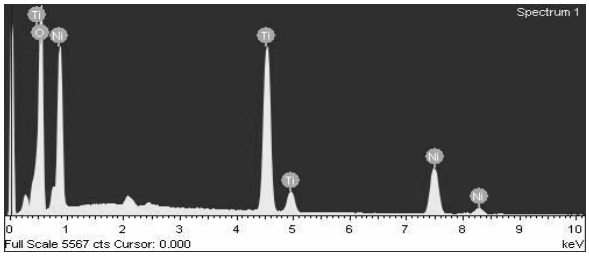

Figure 6. EDAX spectra of $NiTiO_3$ pervoskite formed at 700 ^oC/4 h.

UV-Vis diffuse reflectance spectroscopy (DRS) was used for evaluating the optical response and the determination of band gap of the synthesized powder. The DRS spectrum of $NiTiO_3$ shows the optical characteristics of nano powder in both the UV and visible light region. The DRS spectra reveal two peaks, one at around 440-450 nm and another one at around 740-750 nm. The peak at 448 nm is attributed to the $O^{-2} \rightarrow Ti^{+4}$ charge transfer interaction and the other one 745 nm to $3d^8$ band associated with $Ni^{+2} \rightarrow Ti^{+4}$ charge transfer (CT). Since $NiTiO_3$ samples are heavily coloured, in the present study, the reflection spectra were dominated by the broad intense absorption in the visible region at around 740-750 nm.

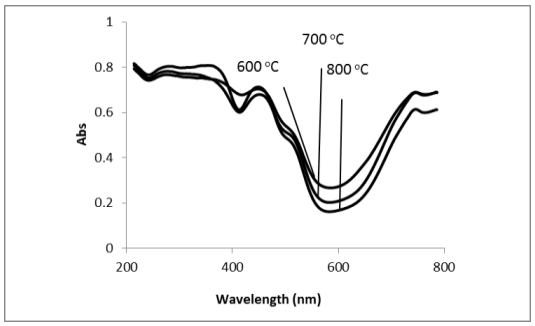

Figure 7. UV-Vis DRS patterns of $NiTiO_3$ at different temperature.

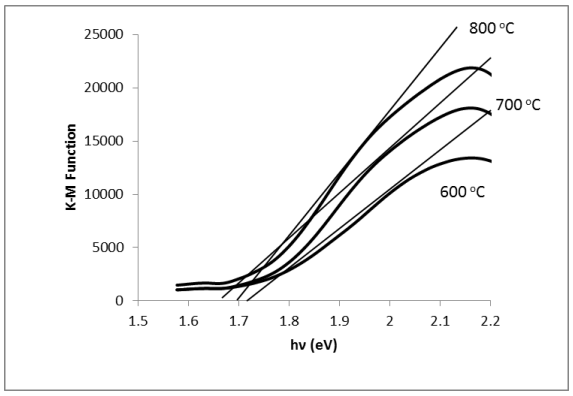

Figure 8. Determination of bandgap values using Kubelka – Munk Function.

Band gap of the samples has been calculated using Tauc plot (35)

$$(h\nu\alpha)^{1/n} = A(h\nu - Eg)$$

where h,ν, Eg, α are the Planck's constant, vibrational frequency, band gap and absorption coefficient respectively. The values of the exponent n denotes the nature of transition in a semiconductor; here it was determined as 1/2 because of direct allowed transition. The acquired diffusion reflectance spectrum is converted to Kubelka- Munk function. Thus, the vertical axis is converted to quantity $F(R\infty)$, which is proportional to the absorption coefficient. The α in the Tauc equation is substituted with $F(R\infty)$. Thus in the actual experiment, the relational expression becomes:

$$(h\nu F(R\infty))^2 = A(h\nu - Eg)$$

Using the Kubelka-Munk function, the $(h\nu F(R\infty))^2$ was plotted against the hν. A line is drawn tangent to the point of inflection on the curve, and the hν value at the point of intersection of the tangent line and the horizontal axis is the band gap Eg value.

The value of band gap for the photo catalyst was calculated and tabulated in Table 2. The lowest band gap is found to be 1.67 eV for the sample calcined at 700 ^oC. The lowest band gap shows that 700 ^oC calcinations temperature is optimum temperature for calcinations of $NiTiO_3$.

A comparison was made, in term of band gap energy of prepared $NiTiO_3$ with other synthesis methods in Table 3. The present study shows that the prepared $NiTiO_3$ is an effective visible light active photocatalyst for the removal of SMX drug from aqueous solutions.

TABLE 2. The band gap energy and particle size of synthesized $NiTiO_3$ at different temperature.

Calcination Temperature	600 ^oC	700 ^oC	800 ^oC
Absorption wavelength (nm)	745	747	742
Band gap (eV)	1.66	1.65	1.67
Crystallite size (nm)	22.04	23.03	32.43

TABLE 3. Comparison of band gap of prepared $NiTiO_3$ with other synthesis methods.

Synthesis method	Band gap(eV)	References
Ultrasound assisted wet chemical processing	3.72	(30)
Pechini	3.02	(29)
Electrospining	2.17	(27)
Sonolysis	2.01	(36)
Modified pechini	1.67	This work

Photocatalytic degradation of SMX

First, non – photocatalytic assay was undertaken to evaluate its isolated influence on the degradation of SMX. In the photolysis, SMX (30 mg L^{-1}) was irradiated for 180 min under visible light irradiation at natural pH (5.5). Results showed that concentration (only 3% degrade) of SMX remains unchanged. The negligible degradation attained by photolysis was expected due to the low SMX molar absorption coefficient above 300 nm.

This means that photolysis is not involved in the degradation of SMX and only the photocatalyst absorbs photons.

As shown in Fig. 9 the SMX (30 mgL^{-1}) aqueous solution can be photocatalytically degraded with different calcined $NiTiO_3$ at natural pH. Under visible light irradiation photo-generated electron and hole can be produced from $NiTiO_3$. And, $^*OH$ active species are produced, which has been reported earlier [37]. These active radical are responsible for SMX degradation. In the mechanism of photocatalytic degradation of SMX reaction involved are as follows:

$$NiTiO_3 + h\nu \rightarrow (e^-_{CB} + h^+_{VB}) \quad \lambda < 800\ nm \quad (1)$$

Equation 1 stated absorption of photons by $NiTiO_3$ and formation of electron/ hole (e^-/h^+) pairs in conduction and valence band.

Eqs. 2, 3 and 4 shows the subsequent formation of hydroxyl radical and its reaction with SMX are :

$$h^+ + H_2O \rightarrow H + {}^*OH \quad (2)$$

$$h^+ + {}^*OH \rightarrow {}^*OH \quad (3)$$

$$(SMX)_{adsorbed} + {}^*OH \rightarrow SMX_{oxidised} \quad (4)$$

It can be observed that, SMX drug was almost 84.25% degraded in 180 min by the NTO calcined at 700 ^oC. While with the sample calcined at 600 ^oC and 800 ^oC, 81.23% and 75.64% degradation was found after 180 min, respectively. The best photocatalytic activity of the NTO perovskite calcined at 700 ^oC was because of its nano particles and low energy band gap as evidenced from our XRD and UV-DRS results respectively which clearly indicate that different annealing temperature may deeply influence the material performance.

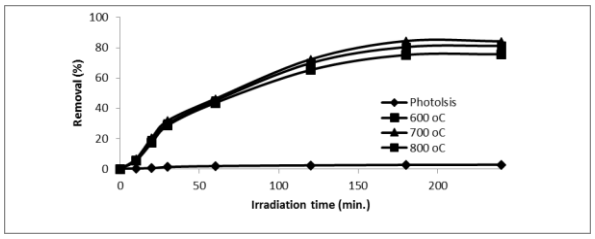

Figure 9. Photolysis and photocatalysis of SMX drug using $NiTiO_3$ obtained at different calcinations temperature (Drug concentration= 30 ppm; catalyst amount 1g1000mL^{-1} pH=5.5).

We also carried out the following controlling experiments with P-25; Degussa TiO_2 and solar irradiation in identical conditions. The P-25; Degussa TiO_2 is very versatile photocatalyst and use of solar light instead of artificial light is important for industrial point of view. Under identical experimental condition, the total photodegradation of the SMX drug reached only 32.65% with widely used P-25 TiO_2 (visible light irradiation) and 87.16% with solar irradiation (NTO photocatalyst) thereby confirming the higher potential of the NTO synthesized in the present study.

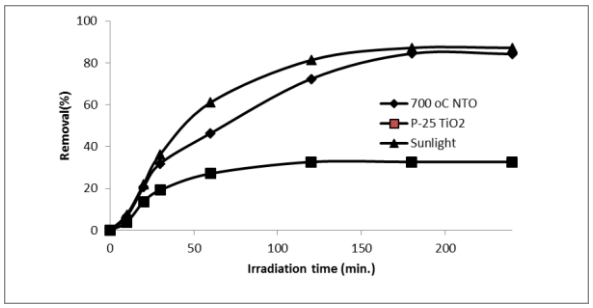

Figure 10. Photocatalysis of SMX drug using $NiTiO_3$ (700 ^oC), P-25 TiO_2 and solar irradiation (Drug concentration= 30 ppm, catalyst amount 1g1000mL^{-1}, pH=5.5)

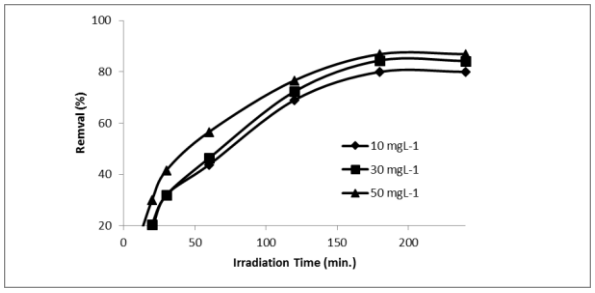

Figure 11. Effect of initial concentration of SMX during SMX removal (catalyst amount 1g1000mL^{-1}, pH=5.5)

The effect of initial SMX concentration on the efficiency of the photocatalytic degradation process was studied and the results are presented in Fig. 11. It can be observed that, SMX degradation increases with the increase in SMX initial concentration. The SMX conversion was 80% with initial concentration of 10 ppm, while conversion was 86.9% with 50 ppm concentration.

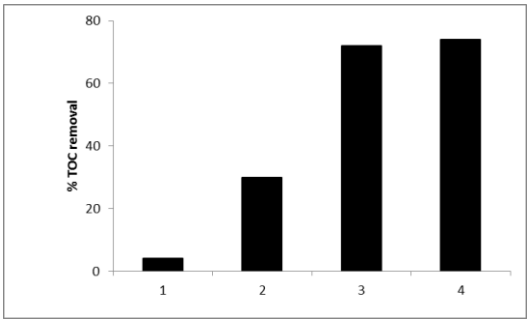

Figure 12. TOC removal in SMX solution obtained by photolysis (1) photocatalysis by P-25 TiO_2 (2) photocatalysis by $NiTiO_3$ under indoor lamp illumination (3) photocatalysis by $NiTiO_3$ in the presence of sunlight (4)

The removal of the initial compound does not indicate that the total mineralization was achieved therefore, a study of the total organic carbon (TOC) quantification was also necessary. As shown in Fig. 12 TOC removal was negligible in photolysis experiment

while under solar light irradiation this rate is highest with $NiTiO_3$ solution .

Kinetic studies of SMX photodegradation

In order to assess the rate of photocatalytic degradation of SMX over NTO powder, the observed SMX degradation results were kinetically analysed by following Langmuir-Hinshelwood rate constant equation [38]. Langmuir-Hinshelwood described the relationship between the initial degradation rate (r) and the initial concentration (C) of the organic substrate for heterogenous photocatalytic degradation. The model can be written as follows.

$$r = -\frac{dC}{dt} = \frac{kK_{abs}C}{1+K_{abs}C} = k_{app}C$$

$$k_{app} = \frac{kK_{abs}C}{1+K_{abs}C}$$

$$\ln\frac{Co}{Ct} = k_{app}\,t$$

C_o(mgL^{-1}) is the initial concentration of SMX, C_t (mgL^{-1}) is the remaining concentration after t (min.) time irradiation, K_{abs} is the Lanmuir – Hinshelwood adsorption equilibrium constant (L^{-1}mg), and k is the pseudo-first-order rate constant relating to NTO surface reaction (mgL^{-1}min^{-1}).

A plot of $\ln(C_o/C_t)$ versus t for all the experiments with different initial concentration of drug is shown in Figure 13 which confirmed the first order reaction. The apparent rate constant of K_{app} can be determined from the slope of the straight line. It is found that K_{app} values for 10 mg L^{-1}, 30 mg L^{-1} and 50 mg L^{-1} concentration of SMX are 9.3 x 10^{-3} min^{-1}, 10.6 x10^{-3} min^{-1} and 11.9 x 10^{-3} min^{-1} respectively.

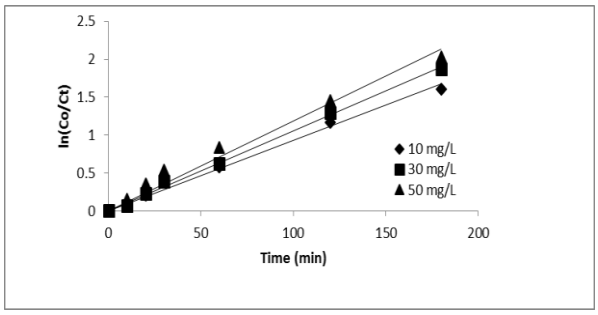

Figure 13. Plots of $\ln(C_o/C_t)$ versus time for $NiTiO_3$ at different initial concentrations of SMX solution

In our work, we also recycled the used NTO by sedimentation for 10 min. Then the long term stability of the NTO was tested by contacting fresh SMX drug solution with regenerated NTO under identical degradation condition. As observed in Fig.14 about 82.32 % degradation efficiency of NTO was achieved in the first run. In the second and third run, 79.68 and 77.21 % degradation of SMX drug was achieved respectively. The results indicate that NTO nanoparticles retain most of their catalytic activity for long time.

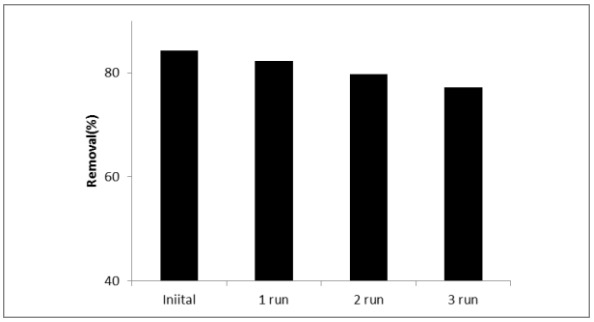

Figure 14. Evaluation of durability of $NiTiO_3$ perovskite.

Intermediate analysis and degradation pathways of SMX

During photocatalytic treatment of SMX, many intermediates were formed and then destructed in the solution simultaneously. Table 4 shows the intermediates detected by an LC/ESI-TOF-MS from $NiTiO_3$ degradation. The intermediates suggested that the probable degradation of SMX leads to form hydroxylated SMX with the mass m/z 269. Based on the above-mentioned intermediates, we suppose that the process of photocatalytic degradation of sulphamethoxole can be divided into the following stage

- Hydroxylation of the aromatic ring
- Cleavage of S-N bond
- Opening of the aromatic ring, and
- Oxidation of aliphatic acids

TABLE 4. CAS number and molecular masses of SMX photocatalytic degrade products

Intermediates	CAS number	m/z
$C_{10}H_{11}N_3O_4S$	114438-33-4	269.3
$C_6H_7NO_3S$	121-57-3	173.1
$C_4H_6N_2O$	1072-67-9	99.1

CONCLUSION

The nanosized $NiTiO_3$ photocatalytic materials are synthesized with Pechini method followed by a suitable calcinations treatment. UV-Vis reflection spectrum showed that NTO nanoparticles have two peaks, one at 448 nm and another one at 745 nm and the band gap is found to be 1.66 eV. The photocatalytic degradation of SMX antibiotic by $NiTiO_3$ photocatalyst under visible irradiation has been reported for the first time, being the pioneer attempt, in this research area. L-H kinetic has been reported on the photodegradation of SMX drug. The regeneration of NTO is found to be successful in removing SMX drug up to 3rd run. Organic intermediates were identified by LC-MS analysis and the major photodegradation products are found to be hydroxylated and S-N cleavage products. The use of $NiTiO_3$ with solar light can offer economically feasibility, high catalytic activity, non toxicity and simplicity of the technological process.

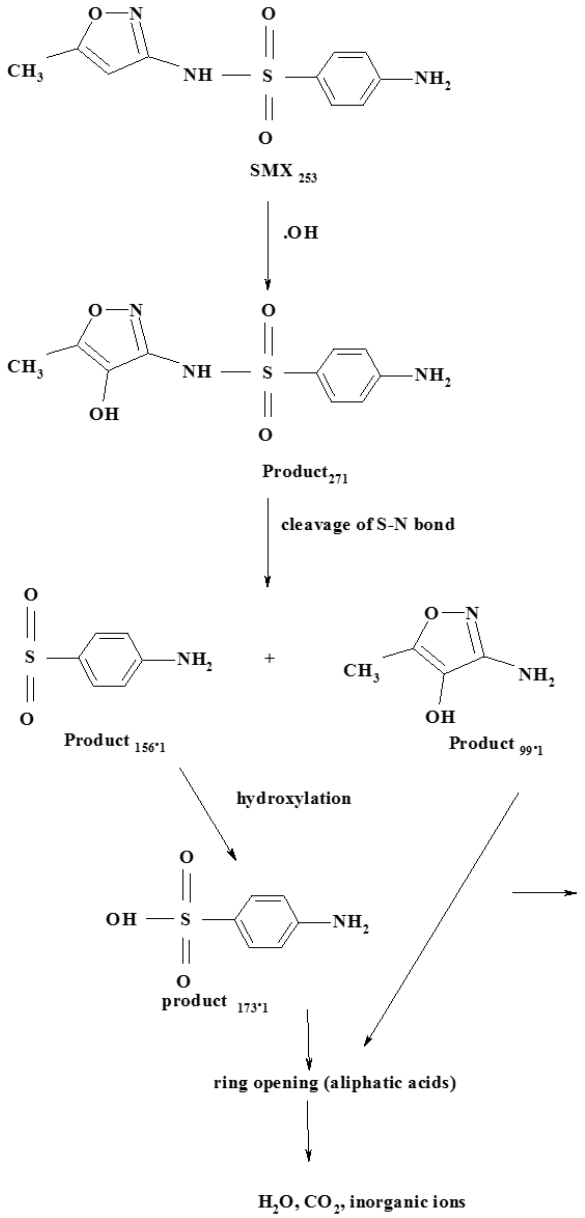

Figure 15. Proposed pathways of the photocatalytic degradation of sulfamethoxazole.

ACKNOWLEDGEMENT

The authors are thankful to University Grant Commission (UGC), New Delhi, India for the financial support in the form of Women Scientist postdoctoral fellowship. We would also like to thank STIC (Sophisticated Test and Instrumentation Centre), Cochin University of Science & Technology for providing experimental support.

REFERENCES

1. Fatta-Kassinos, D., S. Meric, A. Nikolaou, 2011. Pharmaceutical residues in environmental waters and wastewater current state of knowledge and future research, Analitical and Bioanalytical Chemistry, 399 (1): 251-275.
2. Hernando, M.D, M. Ezcua, A.R. Fernandez-Alba, D. Barcelo, 2006. Environmental risk assessment of pharmaceutical residues in wastewater effluents surface water and sediments. Talanta, 69(2): 334-342.
3. Gros, M., M. Petrovic, A.G. Breda, D. Barcelo, 2010. Removal of pharmaceuticals during wastewater treatment and environmental risk assessment using hazard indexes. Environment International , 36(1):15-26.
4. Lekshmi, M., P. Ammini, S. Kumar, M.F. Varela, 2017. The food production environment and the development of antimicrobial resistance in human pathogens of animal origin. Microorganisms, 5: 1-15.
5. 5. Abellan, M.N, B. Bayarri, J. Gimenez, J. Costa, 2007. Photocatalytic degradation of sulfamethoxazole in aqueous suspension of TiO2. Applied Catalysis B-Environmental, 74: 233-241.
6. Hirsch, R., T. Ternes, K. Haberer, K. L. Kratz, 1999. Occurrence of antibiotics in the aquatic environment. Science of the Total Environment, 225: 109-118.
7. Larsson, D.G.J, C. Depedro, N. Paxeus, 2007. Effluent from drug manufactures contains extremely high level of pharmaceuticals. Journal of Hazardous Materials, 148:751-755.
8. Klavarioti, M., D. Mantzavinos, D. Kassinos, 2009. Removal of residual pharmaceutical from aqueous system by advance oxidation process. Environment International, 35: 402-417.
9. Almomani, F.A., M. Shawaqfan, R.R. Bhosale, A. Kumar, 2016. Removal of emerging pharmaceuticals from wastewater by ozone-based advanced oxidation processes. Environmental Progress & Sustainable Energy, 35: 982-995.
10. Lester, Y., D. Avisar, I. Gozlan, H. Mamane, 2011. Removal of pharmecuticals using combination of UV/H2O2/O3 advance oxidation process. Water Science & Technology, 64: 2230-2238.
11. Candido, J.P., S.J. Andrade, A.L. Fonseca, F.S Siva, M.R.A. Silva, M.M. Kondo, 2016. Ibuprofen removal by heterogeneous photocatalysis and ecotoxicological evaluation of the treated solution. Environmental Science and Pollution Research, 23:19911-19920.
12. Chatzitakis, A., C. Berberidou, I. Paspaltsis, G. Kyriakou, T. Sklaviadis, I. Poulios, 2008, Photocatalytic degradation and drug activity reduction of chloramphenicol. Water Research, 42: 386-394.
13. Hu, A., X. Zhang, D. Luong, K.D. Oakes, M.R. Servos, R. Liang, S. Kurdi, P. Peng, Y. Zhou, 2009. Adsorption and photocatalytic degradation kinetics of pharmaceutical by TiO2 nanowires during water treatment. Waste and Biomass Valorization, 1:1-9.
14. Sarkar, S., R. Das, H. Choi, C. Bhattacharjee, 2014. Involvement of process parameter and various modes of application of TiO2 nanoparticles in heterogeneous

photocatalysis of pharmaceutical water- A short review. Royal Society of Chemistry Advance, 100: 57250-57266.
15. Giri, A.S., A.K. Golder, 2014. Fenton, photo-fenton, H2O2 photolysis and TiO2 photocatalysis for dipyrone oxidation: Drug removal, mineralization, biodegradability and degradation mechanism. Industrial & Engineering Chemistry Research, 53: 1351-1358.
16. Kim, S., S.J. Hwang, W. Choi, 2005. Visible light active platinum ion – doped TiO2 photocatalyst. The Journal of Physical Chemistry B, 109 (51): 24260-24267.
17. Kudo, A.K. Omori, H. Kato, 1999. A novel aqueous process for preparation of crystal form controlled and highly crystalline BiVO4 powder from layered vanadates at room temperature and its photocatalytic and photophysical properties. Journal of American Chemical Society, 121: 11459-11467.
18. Tang, J. W., D.F. Wang, Z.G. Zou, J.H. Ye, 2003. Modification of photophysical properties of WO3 by doping different metals. Materials Science Forum, 423:163-166.
19. Sharma, Y.K., M. Kharkwal, S. Uma, R. Nagarajan, 2009. Synthesis and characterization of titanates of the formula MTiO3 (M=Mn,Fe,Co,Ni and Cd) by co-precipitation of mixed metal oxalates. Polyhedron, 28(3): 585-599.
20. Shen, P., J.C. Lofaro, J. Woerner, W.R. White, M.G. Su, D. Oplov, 2013. A photocatalytic activity of hydrogen evolution over Rh doped SrTiO3 prepared by polymerizable complex method. Chemical Engineering Journal, 223: 200-208.
21. Qu, Y., W. Zhou, H. Fu, 2014. Porous cobalt titanate nanorod; A new candidate for visible light driven photocatalytic water oxidation. Chem Cat Chem, 6: 265-270.
22. Qu, Y; W. Zhou, Z. Ren, S. Du, X. Meng, G. Tian, K. Pan, G. Wang, H. Fu, 2012. Facile preparation of porous NiTiO3 nanorods with enhanced visible-light driven photocatalytic performance. Journal of Materials Chemistry, 22: 16471-16476.
23. Yung, D., A. Zikin, I. Hussainova, H. Danninger, E. Badisch, A. Gavrilovic, 2017. Tribological performance of ZrC-Ni and TiC-Ni cerment reinforced PTA hardfacing at elevated temperature. Surface & Coating Technology, 309, 497-505.
24. Della, E.D. Gaspora, A. Martucci, 2015. Sol-Gel thin film for plasmonic gas sensors. Sensors, 15: 16910-16928.
25. Lakshmi, M., A.S. Roy, S. Khasim, M. Faisal, K.C. Sajjan, 2013, Dielectric property of NiTiO3 doped substituted ortho-chloropolyaniline composite. AIP Advan.3, 112: 1-14.
26. Anandan, S., T.L. Villarreal, J. J. Wu, 2015. Sonochemical synthesis of mesoporous NiTiO3 ilmenite nanorods for catalytic degradation of tergitol in water. Industrial & Engineering Chemistry Research, 54(11): 2983-2990.
27. Jing, P., W. Lan, Q. Su, M. Yu, E. Xie, 2014. Visible-light photocatalytic activity of novel NiTiO3 nanowires with rosary like shape. Science of Advanced Materials, 6: 1-7.
28. Lopes, K.P., L.S, Cavalcante, A.Z, Simoes, J.A. Varda, E. Longo, E.R. Leite, 2009. NiTiO3 powder obtained by polymeric precursor method: Synthesis and Characterization. Journal of Alloy and Compound, 468: 327-332.
29. Lin, Y.J., Y.H. Chang, W.D. Yang, B.S. Tsai, 2006. Synthesis and characterization of ilmenite NiTiO3 and $CoTiO_3$ prepared by a modified pechini method. Journal of non Crystaline Solids, 352: 789-794.
30. Moghlada, A., A.S. Unianfar, R. Ashiri, 2015. Facile synthesis of NiTiO3 yellow nanopigments with enhanced solar radiation reflection by an innovative one step method at low temperature. Dyes and Pigments, 123: 92-99.
31. Visser, H., C.E, Dude, W.H, Armstrong, K. Sauer, V. K. Yachandra, 2002. FTIR spectra and normal-mode analysis of a tetranuclear manganese adamantine like complex in two electrochemical prepared oxidation state; Relevance to the oxygen evolving complex of photosystem II. Journal of the American Chemical Society, 124: 11008-11017.
32. Anjana, P.S., M.Th. Sebastian, 2006. Synthesis Characterization and microwave dielectric properties of ATiO3 (A= Co,Mn,Ni) ceramics. Journal of American Ceramic Society, 89: 2114-2117.
33. Vijayalalakashimi, R., V. Rajendran, 2012. Effect of reaction temperature on size and optical properties of NiTiO3 nanoparticles. Eouropean Journal of Chemistry, 9: 282-288.
34. Yuvaraj, S., V.D. Nithya, F.K. Sqiadali, C. Sanjeeviraja, G.S Kalai, S. Arumugam, 2013. Investigation on the temperature dependent electrical and magnetic properties of NiTiO3 by molten salt synthesis. Materials Research Bulletin, 48: 110-116.
35. Lopez, R., R. Gomez, 2012. Band-gap energy estimation from diffuse reflectance measurement on sol-gel commercial TiO2: a comparative study. Journal of sol-gel Science and Technology, 61: 1-7.
36. Pugazhenthiran, N., K. Kaviyarasan, T. Sivasankar, A. Emeline, D. Bahnemann, R.V. Mangalaraja, S. Anandan, 2017. Sonolchemical synthesis of porous NiTiO3 nanorods for photocatalytic degradation of ceftiofur sodium. Ultrasonic Sonochemistry, 35: 342-350:
37. Zhang, J., Y. Nosaka, 2014. Mechanism of the OH radical generation in photocatalysis with TiO2 of different crystalline types. The Journal of Physical Chemistry, 118: 10824-10832.
38. Zonoyz, P.R., A. Niaei, A. Tarjomannejed, 2016. Kinetic modelling of CO oxidation over La1-xAxMn0.6Cu0.4O3 (A=Sr and Ce) nanoperovskie type mixed oxides. International Journal of Environmental Science and Technology, 13: 1665-1674.

Persian Abstract

DOI: 10.5829/ijee.2017.09.01.05

چکیده

نانوذرات اکسید تیتانیوم نیکل (NiTiO3) با دمای پایین در محیط غیر آبی با روش Pechini اصلاح شده با استفاده از اتیلن گلیکول و اسید سیتریک به عنوان پیش ماده های پلیمری سنتز شد. ویژگی های ساختاری و مورفولوژیکی محصولات با استفاده از پراش اشعه ایکس، طیف سنجی مادون قرمز فوریه (FT-IR)، طیف سنجی بازتابی پراکنده UV (UV-DRS)، میکروسکوپ الکترونی اسکن (SEM) و اشعه ایکس پراکنده انرژی طیف سنجی (EDAX). الگوهای پودر XRD نشان داد NiTiO3 rhombohedral بلور به دست آمده در ۷۰۰ درجه سانتیگراد و این کریستالی با دمای افزایش می یابد. تصاویر SEM تخمین زده اند که اندازه دانه NiTiO3 در محدوده ۱۰-۲۵۰ نانومتر باشد. طیف های DRS دو پیک را نشان می دهند، یکی در حدود ۴۴۰-۴۵۰ نانومتر و دیگری در حدود ۷۴۰-۷۵۰ نانومتر. انرژی شکاف باند با استفاده از طرح Tauc محاسبه شد و به ۱،۶۷ eV محاسبه شد. در این مطالعه خواص فتوکاتالیتی NiTiO3 بر روی تخریب داروهای سولفامتوکسازول بررسی شده است که در جای دیگر گزارش نشده است و نتایج نشان می دهد که این مواد مهم در معرض نور خورشید در محدوده نور قابل مشاهده است.